

## Real-time monitoring of calcium sulfate scale removal from RO desalination membranes using Raman spectroscopy



Danielle J. Park<sup>a,\*</sup>, Omkar D. Supekar<sup>a,c</sup>, Alan R. Greenberg<sup>a,b</sup>, Juliet T. Gopinath<sup>c,d</sup>, Victor M. Bright<sup>a</sup>

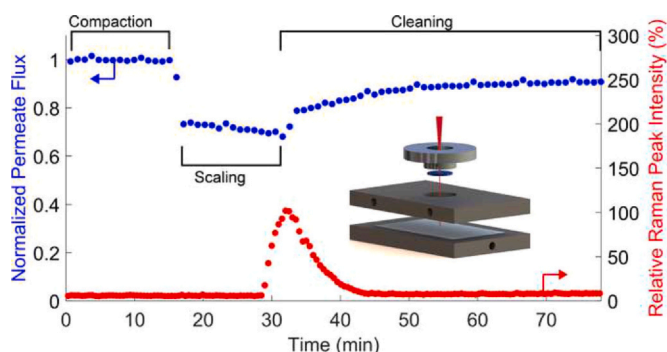
<sup>a</sup> Department of Mechanical Engineering, University of Colorado, Boulder, CO 80309, USA

<sup>b</sup> Membrane Science, Engineering and Technology Center, University of Colorado, Boulder, CO 80309, USA

<sup>c</sup> Department of Electrical, Computer, and Energy Engineering, University of Colorado, Boulder, CO 80309, USA

<sup>d</sup> Department of Physics, University of Colorado, Boulder, CO 80309, USA

### GRAPHICAL ABSTRACT



### ARTICLE INFO

#### Keywords:

Scale removal  
Raman spectroscopy  
RO desalination membrane  
Real-time characterization

### ABSTRACT

Chemical characterization of scaling and removal processes was performed in real time via Raman spectroscopy in a bench-scale reverse osmosis (RO) system. A custom RO cross-flow cell was integrated with a Raman microscope objective, allowing for analysis of localized membrane scaling and scale removal. Permeate flux was also measured to provide a real-time metric for comparison. A commercial flat sheet, thin-film composite reverse osmosis (TFC RO) membrane was scaled using a calcium sulfate ( $\text{CaSO}_4 \cdot \text{H}_2\text{O}$ ) feed solution. Upon  $\text{CaSO}_4$  scale detection, the feed was switched to DI water, which served as a cleaning agent to remove the  $\text{CaSO}_4$  scale from the membrane. In addition to the real-time local (Raman) and global (permeate flux) measurements, membrane samples were characterized post-mortem using Raman spectroscopy, gravimetric analysis and scanning electron microscopy to provide important scaling and scale removal metrics. Results from real-time measurements indicated that changes in Raman intensity were a more sensitive indicator of local scale removal than changes in permeate flux, a standard cleaning performance metric; these findings were corroborated by the post-mortem analyses. Overall, the membrane cleaning experiments showed that Raman spectroscopy provided crucial real-time chemical composition and spatial distribution information, which can inform more effective antiscaling and cleaning strategies.

\* Corresponding author.

E-mail address: [danielle.j.park@colorado.edu](mailto:danielle.j.park@colorado.edu) (D.J. Park).

<https://doi.org/10.1016/j.desal.2020.114736>

Received 18 June 2020; Received in revised form 25 August 2020; Accepted 27 August 2020

0011-9164/ © 2020 Elsevier B.V. All rights reserved.

## 1. Introduction

Reverse osmosis (RO) is the world's leading desalination technology [1], providing much needed clean water not only in semi-arid regions, but also in temperate and coastal locations [2–5]. Reverse osmosis is a high-energy consumption, membrane-based separation process that inevitably results in membrane fouling [1]. Depending on the membrane separation process, fouling components can be classified as inorganic, organic, and microbial [6]. In commercial RO systems, common foulants include inorganic minerals, also known as scale. The concentration of inorganic minerals in the feed increases in the direction of the flow, which is a phenomenon known as concentration polarization [7,8], although in the case of organic foulants present upstream, scale formation may increase in the upstream direction [9]. Due to the blockage that results from scale deposited on the membrane surface, permeate flux decreases such that the feed pressure must be increased to maintain the pre-fouling flux value [10]. In addition, concentration polarization and the resulting scale growth lead to lower permeate quality [11].

The literature indicates that real-time detection of fouling in membrane-based desalination can be an important means to minimize energy consumption and maintenance costs in large-scale desalination plants [12–14] because, in general, membrane cleaning measures are most effective in the early stages of scaling before irreversible damage occurs [6]. Due to the spatial variation in membrane scaling caused by concentration polarization, a real-time sensing technique that provides local detection is needed. In response to this critical need, a number of different methods of scaling/fouling detection have been developed. Ultrasonic time-domain reflectometry (UTDR) [8,15–18], electrical impedance spectroscopy (EIS) [19,20], Raman spectroscopy [21–23], visual observation techniques [24–26], streaming potentials [27,28], magnetic resonance [29] and X-ray imaging [30] are methods that have been used to study membrane fouling in real time. Many of these techniques can also be used to monitor membrane cleaning. For example, Uchymiak et al. [24] demonstrated scale detection and monitoring of scale removal using an ex situ scale observation detector (EXSOD) in a bench-scale reverse osmosis flow cell. Many of these aforementioned fouling detection techniques have successfully been demonstrated in bench-scale, cross-flow cells employing flat-sheet geometry. In general, it is impractical to directly utilize these methods on spiral-wound membrane modules [18]. However, many of these fouling detection techniques can instead be applied to side streams that are diverted from the spiral-wound membrane modules at preferential locations, such as downstream, where concentration polarization increases the chances of early-onset scale formation. While each of these aforementioned techniques offer a different set of advantages and disadvantages, Raman spectroscopy uniquely provides real-time

information regarding chemical composition of the scaling layer. Such chemical information is important for monitoring scale removal, i.e. membrane cleaning, in real time since it can provide a basis for formulating the best cleaning/antiscaling strategy. In particular, in complex feed waters, the timing, dosage, and chemical composition of the cleaning/antiscaling agents must be tailored to the multiple components in the feed water for optimal results [8]. Clearly, customization of the cleaning strategy would benefit from knowledge of the real-time chemical composition of the scale.

In this work, Raman spectroscopy is utilized for the first time to monitor scale removal from an RO membrane during desalination operating conditions. This is performed in real time by monitoring changes in the intensity of the peaks corresponding to the chemical composition of the scalant under the Raman sensor. Here, incident photons from a laser focused onto the membrane surface through an optical window interact with optical phonons in the scale layer to generate inelastically scattered photons [31]. The energy difference between the incident and scattered photons, known as the Raman shift, is specific to the rotational and vibrational transitions of bonds in a molecule. The intensity of Raman shifts corresponding to the scalant provides the means for chemical identification and relative quantification of the extent of the scaling.

We provide a detailed description of the proof-of-concept application of Raman spectroscopy for monitoring the removal of  $\text{CaSO}_4$  scale in a bench-scale RO system.  $\text{CaSO}_4$  was selected as the model scalant in these studies because it is one of the most common scalants encountered in RO desalination [32]. An important component of the cleaning experiments conducted in this work is the comparison between the real-time Raman and permeate flux measurements, the latter constituting a commonly used indicator of membrane cleaning in commercial desalination plants [33]. While real-time changes in permeate flux are an indirect indicator of global scale deposition and removal, Raman spectroscopy provides a direct and chemically specific measurement of changes in a localized region. This initial study highlights the sensitivity and accuracy of the Raman technique and its capability to provide chemical information as a function of cleaning time and membrane location. Ultimately, the Raman methodology described here could lead to the development of improved membrane cleaning techniques.

## 2. Experimental

### 2.1. Reverse osmosis system

A custom-built RO cross-flow cell and supporting system were used to conduct the membrane cleaning experiments. A schematic of the cross-flow cell is shown in Fig. 1, and the RO system diagram is shown

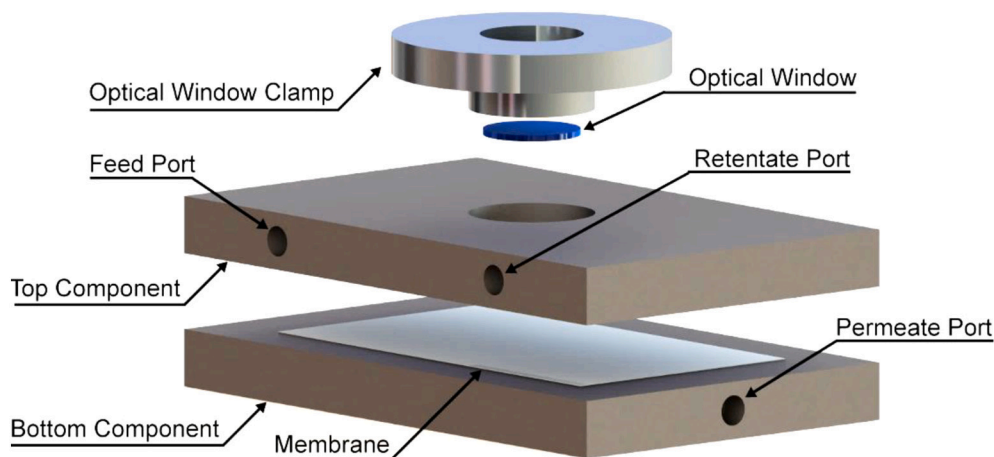


**Fig. 1.** An exploded view of the RO flow cell is shown. The optical window accommodates the Raman microscope objective for real-time acquisition of Raman spectra during desalination. The top component houses the feed and retentate ports, while the bottom component includes the permeate port. The membrane is supported by a stainless steel mesh on the permeate side.

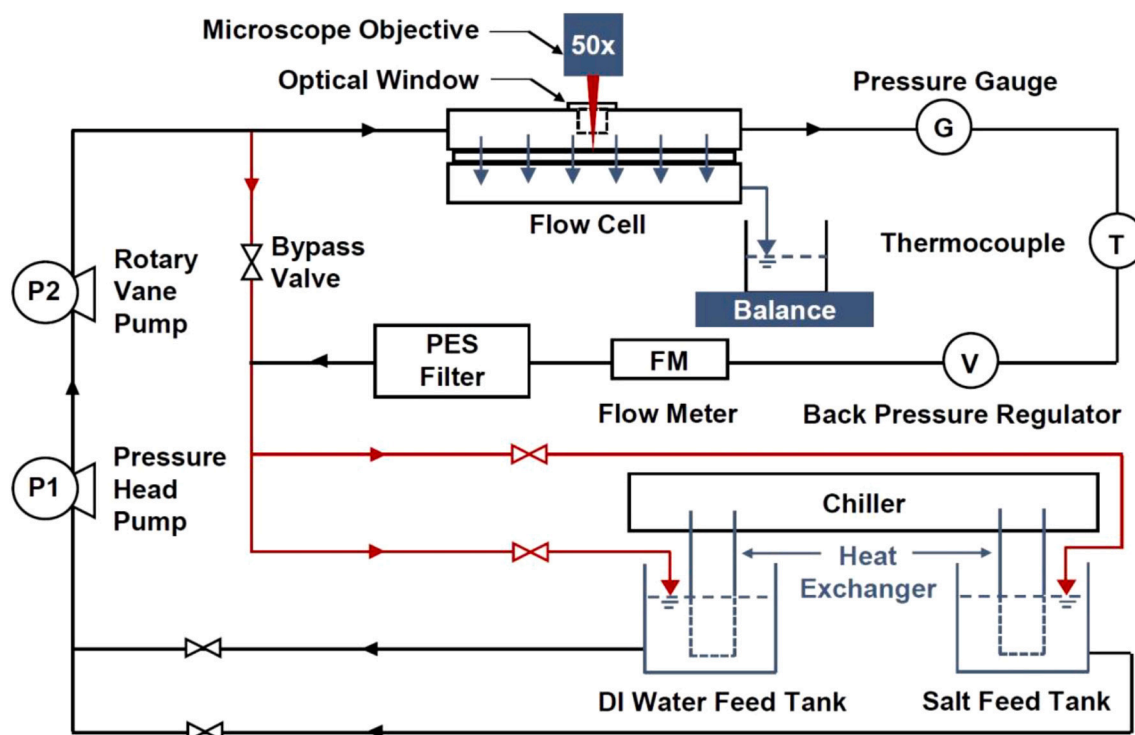


**Fig. 2.** A diagram of the bench-scale RO system features two feed tanks with valves to facilitate the transition between membrane scaling and cleaning. Pressure, temperature, and flow rate were monitored and controlled using a pressure gauge and backpressure regulator, thermocouple and chiller, and flow meter and bypass valve, respectively.

in Fig. 2. The top and bottom components of the flow cell were constructed from 0.625-inch (1.59 cm) thick plates of stainless steel to withstand the high operating pressures. The top component features an inlet (feed) port that injected pressurized feed into the flow cell and flushed the retentate through the outlet (retentate) port. The bottom component is fitted with a stainless steel mesh to support the membrane. To allow for the real-time collection of Raman spectra, the flow cell features an optical window that interfaces with a 50 $\times$  microscope objective (Model N-PLAN L50x/0.50, Leica Germany) of the Raman microscope (Model inVia Reflex, Renishaw). The flow cell was mounted on a custom stage with an adjustable z-axis, and fixed x- and y- axes, and the center of the flow cell was aligned with the Raman microscope.

A high-pressure rotary vane pump (Model TMFRSS051A, Fluid-o-Tech) circulated the feed to the flow cell, and a pressure head pump (Model 3-MD-SC, Little Giant) was used to prevent cavitation. The retentate passed through a pressure gauge (100 Series, NoShok) and a backpressure regulator (Model 12-251B2-44AZ5-72, Neon) which were used to monitor and control the pressure in the flow cell, respectively. The retentate was also passed through a 0.2  $\mu$ m polyether sulfone filter (Model CCS-020-C1B, 0.2  $\mu$ m, Advantec) to filter particulates before it was circulated back into the salt feed tank. The temperature of the feed was monitored using a thermocouple downstream of the flow cell and controlled using a chiller (Model T257P, Thermotek). The bottom component of the flow cell features a port through which permeate water was collected in a beaker and its mass monitored with a precision balance (Model PNX-2002, American Weigh Scales). A flow meter (Model 74C-234G041-421330, King) was used to monitor the flow rate, and a bypass valve (Model SS-1RS4, Swagelok) installed upstream of the flow cell was used for flow rate control. Commercial thin-film composite reverse osmosis (TFC RO) membranes (UTC-73HA, Toray) were used in all of the experiments.

## 2.2. Experimental protocol

The feed used to scale the membranes was a 1.8 g/L solution of

calcium sulfate dihydrate (99% Reagent Plus, Sigma–Aldrich) in DI water. The scaling procedure followed that described in previous studies [21,22]. Typically, CaSO<sub>4</sub> cleaning is conducted using a series of acid and water washes to restore the permeate flux as quickly as possible [6,33]; however, for these experiments, DI water washes were deemed adequate for scale removal (cleaning). Before conducting the scaling and cleaning experiments, all membranes were pretreated by soaking in a solution of 300 mL DI water and 300 mL isopropanol for 30 min to remove any additives. The flow cell was cleaned with DI water and isopropanol, and the RO system was flushed with DI water for 30 min to remove residual scale and any contaminants before each experiment. Soaked membranes were placed in the flow cell and compacted in the RO system with a reservoir of DI water for  $\sim$ 15 h, at a temperature of  $23.5 \pm 0.5$  °C, pressure of  $175 \pm 1$  psi (1.2 MPa), and volumetric flow rate of  $15 \pm 1$  LPH (linear flow rate of 4.2 cm/s). After compaction was completed, the Raman microscope objective was lowered into the optical window, and spectral acquisition was initiated for 15 min with DI water to collect baseline Raman spectra on a compacted, clean membrane. To obtain a Raman signal, the height of the stage was adjusted to focus a 785 nm laser (Model I0785SR0090B-IS1, Innovative Photonic Solutions) on the membrane surface through the objective and optical window. Then, the feed was switched from DI water to calcium sulfate solution to initiate scale formation on the membrane.

A first series of experiments (intensity control) were conducted with the aim of simulating one scaling and cleaning cycle, whereby membranes were scaled so that the normalized CaSO<sub>4</sub> Raman peak intensity exceeded 50% and then cleaned until the CaSO<sub>4</sub> Raman peak intensity returned to baseline values (tests 1–4). A second series of experiments (time control) were then conducted where membranes were scaled for 45 min and partially cleaned for 5 min to focus on monitoring the early stages of cleaning (tests 5–7).

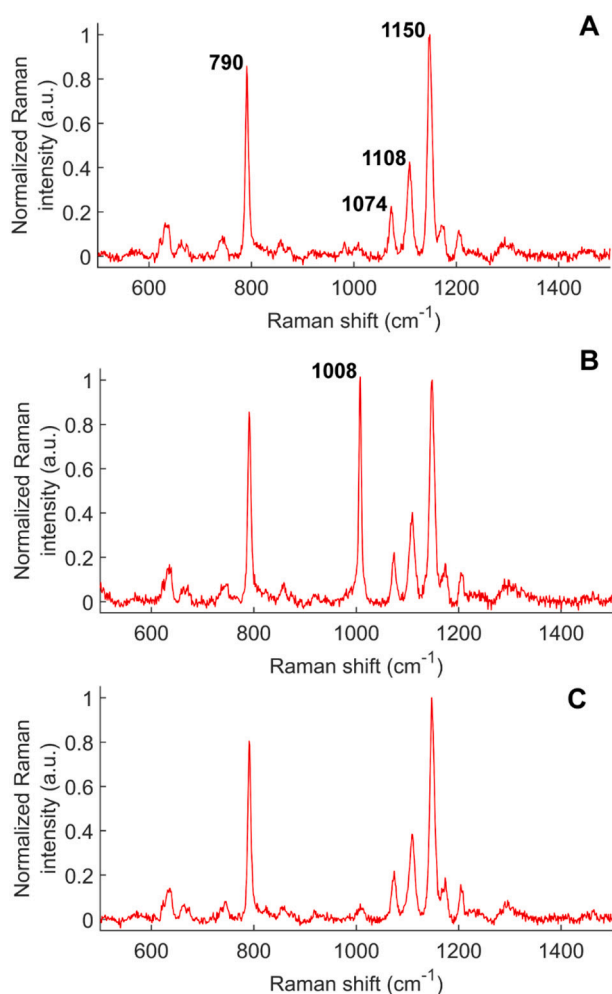


**Fig. 3.** (A) Raman spectra of the TFC RO membrane before the onset of scaling with peaks at  $\sim 790$   $\text{cm}^{-1}$  (C–H deformation), 1074 and 1108  $\text{cm}^{-1}$  ( $\text{SO}_2$  symmetric and antisymmetric stretching), and 1150  $\text{cm}^{-1}$  (C–O–C stretching); (B) as  $\text{CaSO}_4$  scale grows beneath the interrogated region of the membrane, a dominant peak appears at 1008  $\text{cm}^{-1}$ ; and (C) the  $\text{CaSO}_4$  Raman peak intensity decreases as the membrane is cleaned with DI water.

### 2.3. Raman spectra analysis

The Raman spectra of a clean TFC RO membrane is shown in Fig. 3A. During real-time Raman collection, the Raman shift was recorded in the range of 400 to 1500  $\text{cm}^{-1}$  at 20 mW of laser power for each spectrum. For the intensity-controlled experiments, spectral acquisition occurred every 20 s with 10 s of integration time. For the time-controlled experiments, spectral acquisition occurred every 5 s with 5 s of integration time to obtain finer data resolution during the shorter period of cleaning. In post-processing, each spectrum was baseline corrected to remove the effects of fluorescence. The peak at  $\sim 790$   $\text{cm}^{-1}$  results from the C–H bond deforming in an out-of-plane benzene ring, the peaks at 1074 and 1108  $\text{cm}^{-1}$  are the result of symmetric and antisymmetric  $\text{SO}_2$  stretching, respectively, and the peak at 1150  $\text{cm}^{-1}$  appears due to stretching of C–O–C bonds [34]. These are the major peaks observed in the Raman spectrum of polysulfone (PSf). The RO composite membranes are tri-layered with an ultra-thin polyamide layer, an intermediate micro-porous PSf layer, and a polyester support layer. Since the peak at 1150  $\text{cm}^{-1}$  is dominant, the entire Raman spectra was normalized to this peak. When  $\text{CaSO}_4$  crystals (gypsum), whose principal Raman peak occurs at 1008  $\text{cm}^{-1}$  [35], nucleate and grow on the membrane, the membrane and  $\text{CaSO}_4$  peaks are superimposed (Fig. 3B). Then, during membrane cleaning, as  $\text{CaSO}_4$  dissolves and desorbs from the membrane, the peak at 1008  $\text{cm}^{-1}$  decreases (Fig. 3C) because the intensity of the peak is based on volume interactions between the incident photons from the laser and the material of interest ( $\text{CaSO}_4$  scale). Indeed, a significant advantage of the Raman methodology is that the dominant peak wavenumber and peak intensity only depend on chemical composition/structure and relative quantity, respectively, of scale present under the point (area) of laser interrogation.

### 2.4. Post-mortem membrane characterization

#### 2.4.1. Raman spectroscopy performed over a larger sampling area

Post-mortem characterization of cleaned membrane samples from Tests 1–7 was conducted to complement the real-time data and provide more insight into the performance of the Raman sensor during membrane cleaning. The membranes were cut into 4  $\text{cm}^2$  coupons from the upstream, center, and downstream locations (Fig. 4A). The center test coupon encompasses the location where real-time Raman measurements were made during the experiments.

During real-time detection, Raman data were acquired using a fixed Raman microscope objective that was lowered onto the optical window of the cross-flow cell. The resulting sampling area for this detection

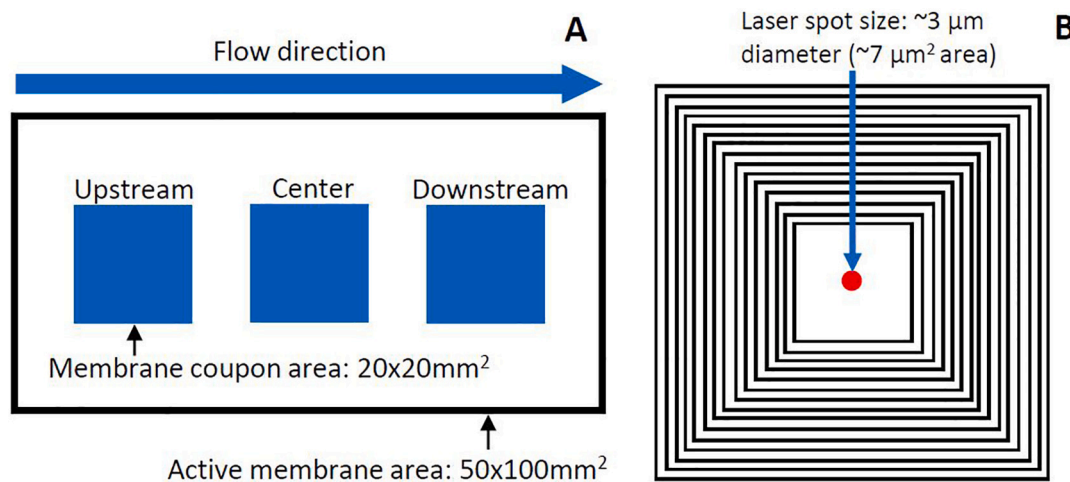


**Fig. 4.** (A) Definition of upstream, center, and downstream locations on the membrane; and (B) For a Raman raster scan, the total sampled area was divided into subspaces to determine the relationship between Raman sampling area and detection capability.

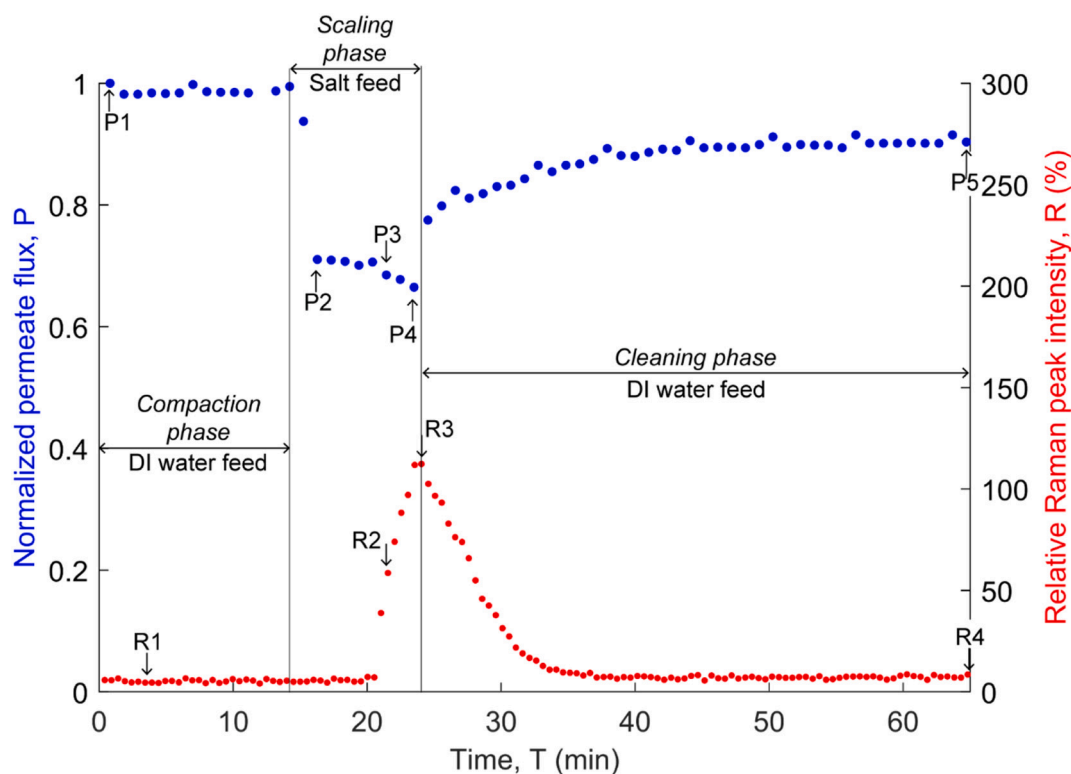


**Fig. 5.** Representative intensity-controlled test result showing the three phases of each test and the permeate flux (**P#**) and Raman (**R#**) data points used to calculate test metrics. **P1**: Initial permeate flux; **P2**: Initial permeate flux with  $\text{CaSO}_4$  feed; **P3**: Permeate flux at scale detection (**R2**); **P4**: Permeate flux at the end of scaling phase; **P5**: Permeate flux at the end of the test; **R1**: Initial baseline Raman peak intensity; **R2**: Scale detection threshold (at least 50% Raman peak intensity); **R3**: Raman peak intensity at cleaning initiation; and **R4**: Raman peak intensity at the end of the test.

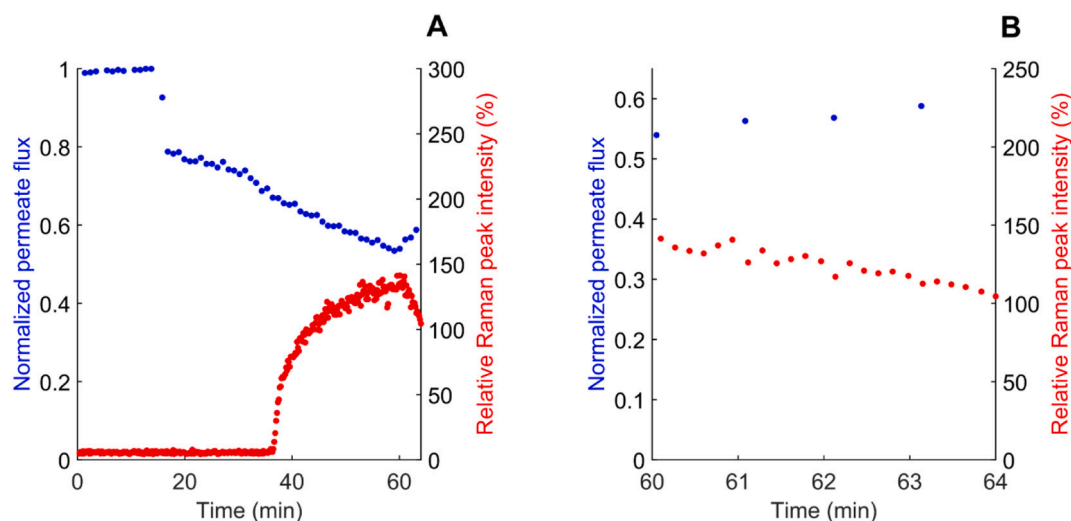


**Fig. 6.** (A) From test 7, a representative progression of relative  $\text{CaSO}_4$  Raman peak intensity is shown for a membrane that was scaled for 45 min and then partially cleaned for 5 min (time-controlled cleaning); corresponding permeate flux values were also determined. (B) The cleaning portion of test 7 is shown in more detail. A consistent, more pronounced decrease in relative Raman peak intensity for  $\text{CaSO}_4$  is observed compared to the increase in permeate flux.

configuration is the spot size of the laser which is  $\sim 3 \mu\text{m}$  in diameter, or  $\sim 7 \mu\text{m}^2$  in area [22]. Given that scale does not form uniformly and cleaning does not necessarily remove scale in a uniform manner, it was desirable to increase the sampling area in order to investigate the relationship between the size of the area sampled and the likelihood of scale detection during/after cleaning. The custom Raman microscope stage used during the cleaning experiments was replaced with the microscope's original high-speed encoded stage, capable of moving the test coupons underneath the fixed microscope objective in precise

increments. For data collection, the stage was programmed to perform a raster scan on the membrane coupon that underwent intensity-controlled cleaning, producing a dataset of  $21 \times 21$  Raman spectra, each spectral acquisition with  $50\text{-}\mu\text{m}$  spacing, spanning a total sampling area of  $1 \text{ mm}^2$  ( $1000 \mu\text{m} \times 1000 \mu\text{m}$ ). For the membrane coupon that underwent time-controlled cleaning, a dataset consisting of  $31 \times 31$  Raman spectra, with  $100\text{-}\mu\text{m}$  spacing between each spectral acquisition, spanning a total sampling area of  $9 \text{ mm}^2$  ( $3000 \mu\text{m} \times 3000 \mu\text{m}$ ) was produced. During data processing, each spectral acquisition site was

**Table 1**

Results from the scaling phase of the experiments. The time of scaling detection was defined as the time taken from salt feed introduction to the time when the CaSO<sub>4</sub> peak reached at least 50% relative Raman peak intensity [21,22].

Test #	Initial permeate flux during scaling [L/m <sup>2</sup> /h]	Time of scaling detection (min)	Duration of scaling (min)	Permeate flux decline at scale detection (%)
1	69.6	15	16	4
2	73.9	27	31	18
3	80.4	7	9	3
4	84.1	6	6	3
5	64.1	30	45	4
6	67.0	10	45	3
7	72.4	23	45	12

**Table 2**

Permeate flux and relative CaSO<sub>4</sub> Raman peak intensity values defined in Fig. 5 are used to calculate test metrics to enable comparison of permeate flux and Raman measurements during the cleaning experiments. **P1**: Initial permeate flux; **P4**: Permeate flux at the end of scaling phase; **P5**: Permeate flux at the end of the test; **R1**: Initial baseline Raman peak intensity; **R3**: Raman peak intensity at cleaning initiation; **R4**: Raman peak intensity at the end of the test; **T<sub>P4</sub>**: Time at P4; **T<sub>P5</sub>**: Time at P5.

Test metric	Formula
Cleaning time (min)	$T_{P5} - T_{P4}$
Permeate flux recovery at end of cleaning (%)	$(P5 - P4) / (P1 - P4) * 100$
CaSO <sub>4</sub> Raman recovery at the end of cleaning (%)	$(R3 - R4) / (R3 - R1) * 100$

**Table 3**

Values of the cleaning metrics for tests 1–7. For the intensity-controlled experiments (tests 1–4), the mean cleaning time was  $64 \pm 7$  min; for the time-controlled experiments (tests 5–7), the mean cleaning time was  $5 \pm 1$  min.

Test #	Start of cleaning, T <sub>P4</sub> (min)	End of cleaning, T <sub>P5</sub> (min)	Permeate flux recovery at T <sub>P5</sub> (%)	Raman recovery at T <sub>R4</sub> (%)
1	32	91	69	97
2	48	118	73	100
3	24	89	73	98
4	21	78	70	99
5	60	64	17	23
6	61	65	15	33
7	60	65	11	37

marked according to the presence or absence of CaSO<sub>4</sub> scale. The presence of scale is defined as a spectral acquisition site that features a Raman spectrum with a relative peak intensity of the dominant peak of CaSO<sub>4</sub> ( $1008 \text{ cm}^{-1}$ )  $> 50\%$  [21,22]. After identifying scale detection at each spectral acquisition site, the total sampled area in the raster scan was partitioned into square subspaces, starting at the center of the raster scan, which consisted of a single Raman spectrum. From the center of the raster scan, the length of the square subspaces consecutively increased by 100  $\mu\text{m}$  and 200  $\mu\text{m}$  for the intensity-controlled and time-controlled samples, respectively, until the largest subspace contained Raman spectra taken from the entire sampled area (Fig. 4B).

#### 2.4.2. Gravimetric measurements

Gravimetric measurements of the membrane coupons were made using a microbalance (ME 235S, Sartorius), and dimensions of the coupons were measured using a digital caliper (DCLA 0605, VINCA). Gravimetric measurements of membrane coupons that underwent scaling and time-controlled cleaning were compared to that of virgin membrane coupons. The virgin membranes were soaked for 30 min in a 1:1 solution of isopropanol and DI water, and then dried before measurement.

#### 2.4.3. Microscopy and X-ray analysis

SEM (scanning electron microscopy) was conducted on membrane samples that underwent both intensity-controlled and time-controlled cleaning. After the gravimetric measurements in Section 2.4.2 were completed, the samples were sputter-coated with 9 nm of gold to prevent excessive charging during imaging. EDX (Energy dispersive X-ray spectroscopy) was conducted on membrane coupons that were cleaned 20+ min to determine whether any residual scale was present.

### 3. Results and discussion

#### 3.1. Real-time metrics

The peak intensity of CaSO<sub>4</sub> was recorded over the duration of each test to assess the performance of the Raman sensor in comparison to permeate flux, a standard membrane performance metric. After the pretreatment and compaction described in Section 2.2, each test begins with an initial 15 min of DI water compaction to characterize the baseline value of the CaSO<sub>4</sub> Raman peak intensity before the salt feed is introduced. Membranes in the intensity-controlled tests (#1–4, Fig. 5) were scaled until the CaSO<sub>4</sub> Raman peak intensity exceeded at least 50% [21,22] and were cleaned until the peak intensity returned to the baseline value (20+ min); membranes in the time-controlled tests (#5–7, Fig. 6) were scaled for 45 min then cleaned for 5 min.

When the salt feed is introduced in both the intensity-controlled and time-controlled tests, the permeate flux initially decreases while the CaSO<sub>4</sub> Raman peak intensity remains at a baseline value. This initial decrease in permeate flux is primarily due to the increased osmotic pressure from the salt concentration in the feed solution. These two different responses to the increased feed concentration indicate that the CaSO<sub>4</sub> Raman peak intensity is not affected by concentration polarization. After the initial decline, the permeate flux continues to decrease due to the combined effects of concentration polarization, compaction, and scale formation. The sensitivity of the real-time Raman and flux measurements can be considered in the context of the degree of the respective changes and the time frame over which they occur. While permeate flux is sensitive to changes in concentration polarization, it does not provide clear information about the onset of scaling. In contrast, the CaSO<sub>4</sub> Raman peak intensity has been shown to be more sensitive to changes on the membrane surface than permeate flux for real-time detection of scaling via specific chemical and spatial information [21]. Despite some scatter in the data, this assertion is supported by the results presented in Table 1 that show low values of permeate flux decline relative to the 50% increase in the Raman peak intensity. The relatively high values of permeate flux decline at Raman scale-detection exhibited in tests 2 and 7 may well reflect somewhat higher levels of scaling elsewhere in the membrane. The variation in time of scaling detection, which ranged from 6 to 30 min, is partly influenced by variations in initial permeate flux values during RO system operation. Since boundary layer concentration on the feed side of the membrane is related to permeate flux (along with other factors such as crossflow velocity, temperature and pressure) [13], scaling detection times for lower initial permeate fluxes tend to be longer because a lower flux leads to lower salt concentration on the feed side of the membrane.

The higher sensitivity in the response of the Raman sensor to scale formation compared to changes in permeate flux is also observed in the response to cleaning. The following test metrics are defined in Table 2 and presented in Table 3: cleaning time, permeate flux recovery at the end of cleaning, and CaSO<sub>4</sub> Raman recovery at the end of cleaning. The permeate flux recovery quantifies the increase in permeate flux attributed to cleaning as compared to the initial permeate flux. The Raman recovery quantifies the extent to which the Raman peak intensity returns to the initial baseline peak intensity values (R1 in Fig. 5) from the maximum peak intensity (R3 in Fig. 5) as a result of cleaning. For example, a Raman recovery of 100% indicates that after cleaning, the Raman peak intensity has completely returned to the baseline value. A

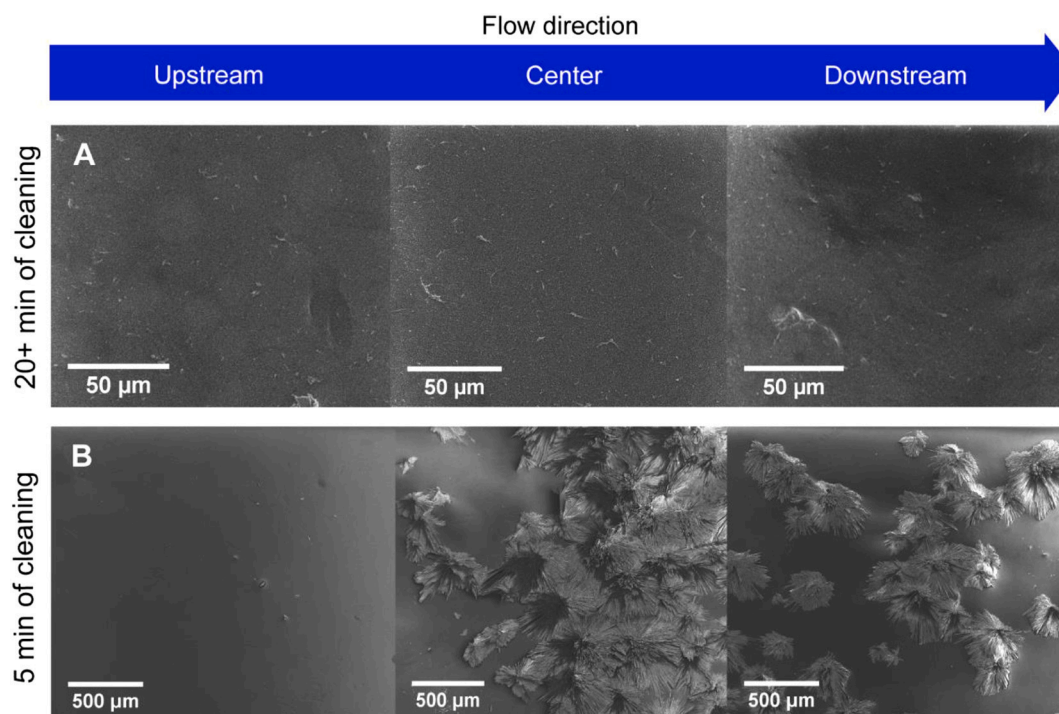


**Fig. 7.** SEM images of upstream, center, and downstream membrane coupons from (A) membranes after 20+ min of cleaning (intensity-controlled cleaning), and (B) membranes cleaned for 5 min (time-controlled cleaning). Membranes that underwent intensity-controlled cleaning show evidence of some residual scale, and membranes that underwent time-controlled cleaning show significantly more scale than those subjected to intensity-control cleaning.

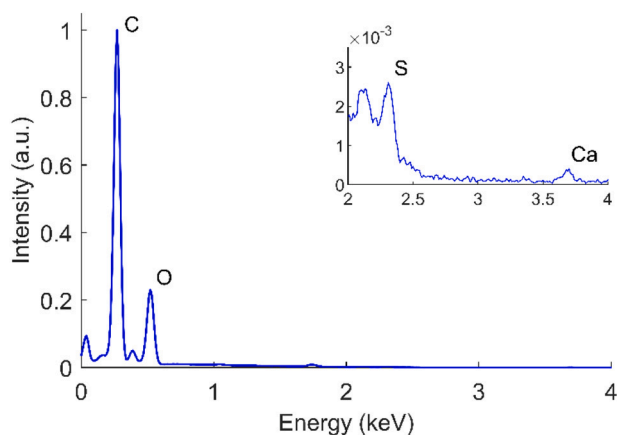


**Fig. 8.** An EDX analysis is shown of an upstream membrane coupon taken from a scaled membrane cleaned for at least 20 min. The inset shows trace amounts of calcium and sulfur compared to the much larger carbon and oxygen peaks.

sensitive method of monitoring membrane cleaning is desirable in enabling plant operators to quickly determine whether a cleaning or antiscalant regimen is lessening or worsening scale formation to avoid further damage to the membrane [36]. Results from the intensity-controlled cleaning experiments (tests 1–4) show that for a mean permeate flux recovery of  $71.7 \pm 1.7\%$ , the corresponding mean Raman recovery is  $99.0 \pm 1.0\%$ . For the time-controlled cleaning experiments (tests 5–7), results show that for a mean permeate flux recovery of  $14.0 \pm 3.1\%$ , the corresponding mean Raman recovery is  $31.1 \pm 7.1\%$ . It should be noted that the permeate flux recovery is not only due to dissolution of scale by the DI water feed, but also a rapid, initial decrease in osmotic pressure when the feed is switched from salt to DI water. Therefore, the results show the higher sensitivity of the Raman response compared to the changes in permeate flux due to scale removal. Results from tests 1–4 show Raman recoveries  $> 95\%$  that

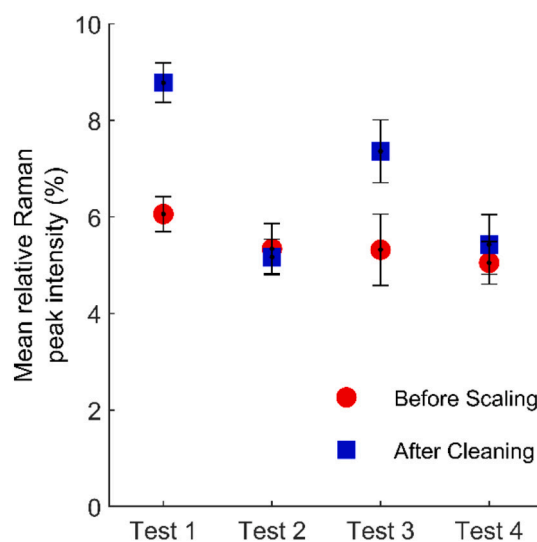


**Fig. 9.** Comparison between mean relative  $\text{CaSO}_4$  Raman peak intensity values before scaling and after cleaning for tests 1–4. The slight increase in the Raman intensity after cleaning in tests 1 and 3 suggests the presence of residual scale.

were achieved well before complete flux recovery, suggesting a more rapid, local Raman response to scale removal as compared to the permeate flux. However, it is also important to again note that the difference in the Raman and permeate flux responses to cleaning is also influenced by differences in the inherent characteristics of local and global measurements. The former reflects the conditions at a small, localized area while the latter considers the possibility of variable conditions across the entire active membrane surface area. This important consideration is addressed in Section 3.3.

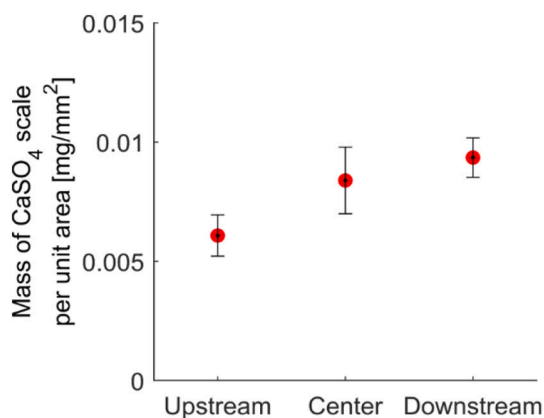


Fig. 10. During scaling, scale formation is greater downstream due to effects of concentration polarization. Gravimetric measurements of upstream, center, and downstream membrane coupons from time-controlled cleaning experiments show a pattern of increased mass in the downstream region. These results suggest a relatively uniform removal of scale in the early stages of cleaning.

### 3.2. Post-mortem characterization

Along with permeate flux recovery as a measure of membrane cleaning, post-mortem visual observation has also been employed [13,15–17]. To provide additional comparison with the real-time Raman metrics, representative scanning electron microscopy (SEM) images of the upstream, center, and downstream membrane coupons from the intensity-controlled and time-controlled experiments are shown in Fig. 7A and B, respectively. For the upstream, center, and downstream locations, the micrographs in Fig. 7 indicate evidence of residual scale on the membrane cleaned for 20+ min while there is clear evidence of CaSO<sub>4</sub> scale remaining on the membrane cleaned for 5 min. These results are consistent with those in Figs. 5 and 6, which indicate that the Raman intensity under the sensor in the center of the membrane has clearly returned to or is very close to the baseline in the former and is well above the baseline value in the latter.

Additional energy-dispersive X-ray spectroscopy (EDX) characterization of an upstream membrane coupon cleaned for 20+ min (Fig. 7A) shows trace amounts of calcium and sulfur, and an abundance of carbon and oxygen (Fig. 8).

The sulfur and oxygen peaks may stem from either residual CaSO<sub>4</sub> scale or the PSf support, and the carbon peak stems from the TFC RO membrane. However, it is the trace amounts of calcium that strongly

support that some small amount of residual scale was present in the corresponding micrograph (Fig. 7A). These EDX results showing possible residual scale are consistent with the CaSO<sub>4</sub> Raman peak intensity not quite returning to the baseline value for two out of the four experiments (tests 1–4; Fig. 9). This result is consistent with findings by Uchymiak et al. [24] who monitored scale growth using a real-time visual technique during an experiment with subsequent scaling, scale dissolution, then rescaling phases. Uchymiak reports that after visually confirming the removal of scale and achieving complete permeate flux recovery, a higher surface crystal number density was observed on the rescaled membrane as compared to the initially scaled membrane. This indicates the possibility of incomplete scale removal even with complete permeate flux recovery and visual confirmation of cleaning. In comparison to visual techniques such as that employed by Uchymiak et al., Raman spectroscopy may provide improved accuracy and sensitivity when monitoring the extent of cleaning.

Gravimetric measurements were made on membranes from tests 5–7 because they were partially cleaned and so had sufficient CaSO<sub>4</sub> scale available for analysis. After 5 min of cleaning, the mass of remaining CaSO<sub>4</sub> is greatest downstream and least in the upstream region (Fig. 10). These results indicate the expected overall pattern of scale removal from the membrane during the initial stages of cleaning with DI water.

### 3.3. Expanded Raman sampling area

As previously noted, the Raman detection methodology for both scaling and cleaning utilizes point measurements. Specifically, the length scales of the Raman laser spot-size, CaSO<sub>4</sub> crystallites, and active membrane area are on the order of 10<sup>-3</sup> mm (Fig. 4B), 10<sup>-1</sup> mm (Fig. 7), and 10<sup>2</sup> mm (Fig. 4A), respectively. Clearly, the laser interrogates an area that is only a fraction of a CaSO<sub>4</sub> crystallite and an orders-of-magnitude smaller fraction of the entire membrane surface. In the present study, these length-scale differences require consideration of the possibility of a false negative during the real-time, fixed-point sampling of the membrane during cleaning, i.e., a no-scaling (clean) signal when scaling is still present at other nearby non-sampled locations. Thus, an alternate, post-mortem sampling strategy that could interrogate a larger portion of the membrane was explored. Raman raster scans spanning a total surface area of 1 × 1 mm<sup>2</sup> and 3 × 3 mm<sup>2</sup> were conducted for representative membranes that underwent intensity-controlled and time-controlled cleaning, respectively. The raster scans consisted of discrete sampling points that were separated by 50 μm for coupons from intensity-controlled cleaning tests and 100 μm

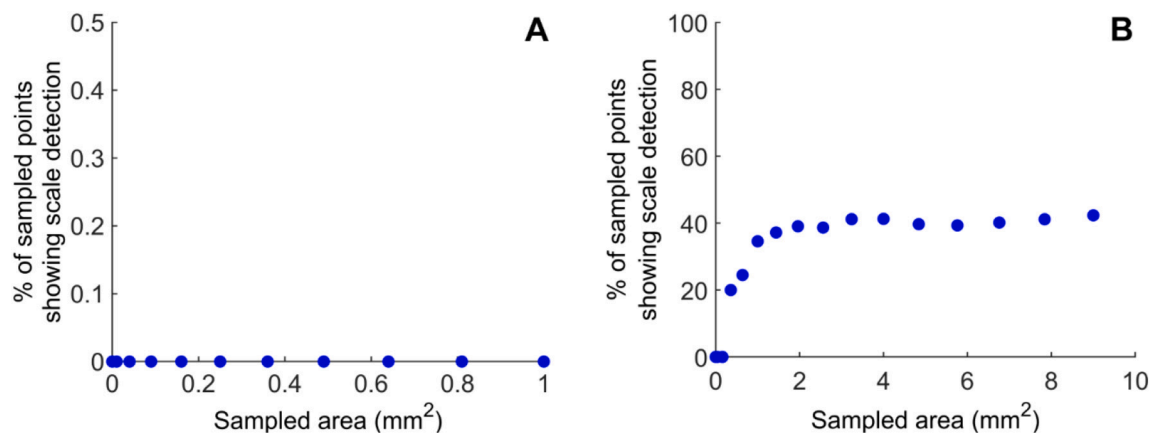


Fig. 11. The percentage of Raman-sampled points indicating the presence of scale is determined for increasing subspaces of the sampled area from representative samples from (A) intensity-controlled, and (B) time-controlled cleaning. The membranes that underwent intensity-controlled cleaning show the absence of measurable scale (i.e. relative CaSO<sub>4</sub> Raman peaks in Raman spectra of sampled sites did not exceed detection threshold of 50%), independent of the area sampled. Membranes that underwent time-controlled cleaning show an initial increase in scale detection with increasing sampled area that becomes relatively constant at ~40%.

from the time-controlled cleaning tests. The raster scan for the intensity-controlled cleaning membrane sample was performed with a higher resolution of 50  $\mu\text{m}$  spacing and smaller total area of  $1 \times 1 \text{ mm}^2$  compared to that of the time-controlled sample because other metrics, such as SEM imaging, indicated that negligible scale was present on the membranes cleaned via the intensity-control procedure. The percentage of sampled points indicating the presence of scale was determined as a function of sampled area (Fig. 11). These analyses were conducted using representative membrane samples from the downstream location.

Results for the intensity-controlled tests (Fig. 11A) indicate the absence of measurable scale independent of the area sampled. In the time-controlled cleaning analysis (Fig. 11B), the percentage of sampled points that indicate scaling detection increases from a sampled area of about 7  $\mu\text{m}^2$  (laser spot-size area) to 9  $\text{mm}^2$  at which the scaling detection percentage becomes relatively constant at  $\sim 40\%$ . The x-axes of Fig. 11A and B both begin at 0% of sampled points showing scale detection because during post-mortem Raman raster scanning, the center of the scan area does not precisely coincide with the location of the real-time point detection. The differences shown in Fig. 11A and B are consistent with almost complete scale removal for the intensity-controlled cleaning and incomplete scale removal for the short, time-controlled cleaning. They also show that there may be an optimal sampling area during cleaning that is large enough to capture the spatial variation in scale distribution, but small enough to facilitate Raman sensor design such as required laser power and scanning speed. Additional factors that must be considered are the size and distribution of the scalant(s), cleaning protocol, and Raman detection thresholds. Overall, these results indicate the necessity to carefully consider sampling strategies and how they affect the accuracy of the real-time Raman scale-detection methodology. Comprehensive study of these aspects comprises the next phase of the work, which we anticipate will provide insights for methodology optimization.

#### 4. Conclusions

This study utilizes real-time Raman spectroscopy to quantify  $\text{CaSO}_4$  scale removal during membrane cleaning in a bench-scale cross-flow RO system. The experiments consisted of an initial scaling phase followed by an in-situ cleaning phase. The prominent  $\text{CaSO}_4$  Raman peak at  $1008 \text{ cm}^{-1}$  consistently increased as scale formed and subsequently decreased as  $\text{CaSO}_4$  dissolved during cleaning using DI water. Compared to the corresponding real-time permeate flux measurements, Raman spectroscopy was more responsive to local conditions during membrane cleaning. The real-time data are supported by microscopic, X-ray, and gravimetric post-mortem characterizations. In addition, post-mortem Raman analysis provided a basis for an improved real-time sampling strategy. A significant advantage of Raman spectroscopy is the ability to provide spatial and chemical information regarding scale formation and removal. Such real-time information could ultimately enable improved cleaning strategies and thus more efficient membrane-based desalination.

#### CRedit authorship contribution statement

**Danielle Park:** Methodology, investigation, visualization, writing – original draft; **Omkar Supekar:** Conceptualization, methodology, supervision, visualization, writing – review & editing; **Alan Greenberg:** Funding acquisition, conceptualization, methodology, supervision, writing – review & editing; **Juliet Gopinath:** Funding acquisition, methodology, supervision, writing – review & editing; **Victor Bright:** Funding acquisition, methodology, supervision, writing – review & editing.

#### Declaration of competing interest

The authors declare that they have no known competing financial interests or personal relationships that could have appeared to influence the work reported in this paper.

#### Acknowledgements

The authors gratefully acknowledge the support of this work by NSF (National Science Foundation) through awards, CBET 1826542 and CBET 1338154. The authors also acknowledge support for the early stages of this work from the Membrane Science, Engineering and Technology Center (NSF IUCRC Award IIP 1624602) at the University of Colorado Boulder. The authors thank Dr. Joseph Swisher (EPRI) for helpful technical discussions. The authors also appreciate the assistance of flow cell fabrication provided by Dragan Mejcic and the Colorado Shared Instrumentation in Nanofabrication and Characterization for access to SEM/EDX instrumentation.

#### References

- [1] K.P. Lee, T.C. Arnot, D. Mattia, A review of reverse osmosis membrane materials for desalination—development to date and future potential, *J. Membr. Sci.* 370 (2011) 1–22, <https://doi.org/10.1016/j.memsci.2010.12.036>.
- [2] B.J. Mariñas, R.E. Selleck, Reverse osmosis treatment of multicomponent electrolyte solutions, *J. Membr. Sci.* 72 (1992) 211–229, [https://doi.org/10.1016/0376-7388\(92\)85050-S](https://doi.org/10.1016/0376-7388(92)85050-S).
- [3] Y. Mogheir, A.A. Foul, A.A. Abuhabib, A.W. Mohammad, Large-scale brackish water desalination plants in Gaza strip: assessments and improvements, *Journal of Water Reuse and Desalination; London*. 3 (2013) 315–324 <http://dx.doi.org.colorado.idm.oclc.org/10.2166/wrd.2013.089>.
- [4] D.P. Rico, M.F.C. Arias, A reverse osmosis potable water plant at Alicante University: first years of operation, *Desalination*. 137 (2001) 91–102, [https://doi.org/10.1016/S0011-9164\(01\)00207-7](https://doi.org/10.1016/S0011-9164(01)00207-7).
- [5] V.J. Shah, C.V. Devmurari, S.V. Joshi, J.J. Trivedi, A. Prakash Rao, P.K. Ghosh, A case study of long-term RO plant operation without chemical pretreatment, *Desalination*. 161 (2004) 137–144, [https://doi.org/10.1016/S0011-9164\(04\)90049-5](https://doi.org/10.1016/S0011-9164(04)90049-5).
- [6] S.S. Madaeni, S. Samieirad, Chemical cleaning of reverse osmosis membrane fouled by wastewater, *Desalination*. 257 (2010) 80–86, <https://doi.org/10.1016/j.desal.2010.03.002>.
- [7] P.L.T. Brian, Concentration polarization in reverse osmosis desalination with variable flux and incomplete salt rejection, *Ind. Eng. Chem. Fund.* 4 (1965) 439–445, <https://doi.org/10.1021/i160016a014>.
- [8] Z. Zhang, V.M. Bright, A.R. Greenberg, Use of capacitive microsensors and ultrasonic time-domain reflectometry for in-situ quantification of concentration polarization and membrane fouling in pressure-driven membrane filtration, *Sensors Actuators B Chem.* 117 (2006) 323–331, <https://doi.org/10.1016/j.snb.2005.11.016>.
- [9] F. Tang, H.-Y. Hu, L.-J. Sun, Y.-X. Sun, N. Shi, J.C. Crittenden, Fouling characteristics of reverse osmosis membranes at different positions of a full-scale plant for municipal wastewater reclamation, *Water Res.* 90 (2016) 329–336, <https://doi.org/10.1016/j.watres.2015.12.028>.
- [10] L.N. Sim, J. Gu, H.G.L. Coster, A.G. Fane, Quantitative determination of the electrical properties of RO membranes during fouling and cleaning processes using electrical impedance spectroscopy, *Desalination*. 379 (2016) 126–136, <https://doi.org/10.1016/j.desal.2015.11.006>.
- [11] K. Madireddi, R.B. Babcock, B. Levine, J.H. Kim, M.K. Stenstrom, An unsteady-state model to predict concentration polarization in commercial spiral wound membranes, *J. Membr. Sci.* 157 (1999) 13–34, [https://doi.org/10.1016/S0376-7388\(98\)00340-8](https://doi.org/10.1016/S0376-7388(98)00340-8).
- [12] A. Jiang, H. Wang, Y. Lin, W. Cheng, J. Wang, A study on optimal schedule of membrane cleaning and replacement for spiral-wound SWRO system, *Desalination*. 404 (2017) 259–269, <https://doi.org/10.1016/j.desal.2016.11.025>.
- [13] K.G. Tay, L. Song, A more effective method for fouling characterization in a full-scale reverse osmosis process, *Desalination*. 177 (2005) 95–107, <https://doi.org/10.1016/j.desal.2004.11.017>.
- [14] J.-W. Nam, J.-Y. Park, J.-H. Kim, S. Kwon, K. Chon, E.-J. Lee, H.-S. Kim, A. Jang, The evaluation on concentration polarization for effective monitoring of membrane fouling in seawater reverse osmosis membrane system, *J. Ind. Eng. Chem.* 20 (2014) 2354–2358, <https://doi.org/10.1016/j.jiec.2013.10.012>.
- [15] A.P. Mairal, A.R. Greenberg, W.B. Krantz, L.J. Bond, Real-time measurement of inorganic fouling of RO desalination membranes using ultrasonic time-domain reflectometry, *J. Membr. Sci.* 159 (1999) 185–196, [https://doi.org/10.1016/S0376-7388\(99\)00058-7](https://doi.org/10.1016/S0376-7388(99)00058-7).
- [16] G. Mizrahi, K. Wong, X. Lu, E. Kujundzic, A.R. Greenberg, J. Gilron, Ultrasonic sensor control of flow reversal in RO desalination. Part 2: mitigation of calcium carbonate scaling, *J. Membr. Sci.* 419 (420) (2012) 9–19, <https://doi.org/10.1016/j.memsci.2012.05.026>.

- [17] X. Lu, E. Kujundzic, G. Mizrahi, J. Wang, K. Cobry, M. Peterson, J. Gilron, A.R. Greenberg, Ultrasonic sensor control of flow reversal in RO desalination—part 1: mitigation of calcium sulfate scaling, *J. Membr. Sci.* 419–420 (2012) 20–32, <https://doi.org/10.1016/j.memsci.2012.05.027>.
- [18] K.D. Cobry, Z. Yuan, J. Gilron, V.M. Bright, W.B. Krantz, A.R. Greenberg, Comprehensive experimental studies of early-stage membrane scaling during nanofiltration, *Desalination*. 283 (2011) 40–51, <https://doi.org/10.1016/j.desal.2011.04.053>.
- [19] A. Antony, T. Chilcott, H. Coster, G. Leslie, In situ structural and functional characterization of reverse osmosis membranes using electrical impedance spectroscopy, *J. Membr. Sci.* 425–426 (2013) 89–97, <https://doi.org/10.1016/j.memsci.2012.09.028>.
- [20] J.M. Kavanagh, S. Hussain, T.C. Chilcott, H.G.L. Coster, Fouling of reverse osmosis membranes using electrical impedance spectroscopy: measurements and simulations, *Desalination*. 236 (2009) 187–193, <https://doi.org/10.1016/j.desal.2007.10.066>.
- [21] O.D. Supekar, J.J. Brown, A.R. Greenberg, J.T. Gopinath, V.M. Bright, Real-time detection of reverse-osmosis membrane scaling via Raman spectroscopy, *Ind. Eng. Chem. Res.* (2018) 16021–16026, <https://doi.org/10.1021/acs.iecr.8b01272>.
- [22] O.D. Supekar, D.J. Park, A.R. Greenberg, J.T. Gopinath, V.M. Bright, Real-time detection of early-stage calcium sulfate and calcium carbonate scaling using Raman spectroscopy, *J. Membr. Sci.* 596 (2020) 117603, <https://doi.org/10.1016/j.memsci.2019.117603>.
- [23] T. Virtanen, S.-P. Reinikainen, M. Kögler, M. Mänttari, T. Viitala, M. Kallioinen, Real-time fouling monitoring with Raman spectroscopy, *J. Membr. Sci.* 525 (2017) 312–319, <https://doi.org/10.1016/j.memsci.2016.12.005>.
- [24] M. Uchymiak, A. Rahardianto, E. Lyster, J. Glater, Y. Cohen, A novel RO ex situ scale observation detector (EXSOD) for mineral scale characterization and early detection, *J. Membr. Sci.* 291 (2007) 86–95, <https://doi.org/10.1016/j.memsci.2006.12.038>.
- [25] J.C. Chen, Q. Li, M. Elimelech, In situ monitoring techniques for concentration polarization and fouling phenomena in membrane filtration, *Adv. Colloid Interf. Sci.* 107 (2004) 83–108, <https://doi.org/10.1016/j.cis.2003.10.018>.
- [26] H. Li, A.G. Fane, H.G.L. Coster, S. Vigneswaran, Direct observation of particle deposition on the membrane surface during crossflow microfiltration, *J. Membr. Sci.* 149 (1998) 83–97, [https://doi.org/10.1016/S0376-7388\(98\)00181-1](https://doi.org/10.1016/S0376-7388(98)00181-1).
- [27] M. Nyström, A. Pihlajamäki, N. Ehsani, Characterization of ultrafiltration membranes by simultaneous streaming potential and flux measurements, *J. Membr. Sci.* 87 (1994) 245–256, [https://doi.org/10.1016/0376-7388\(94\)87031-4](https://doi.org/10.1016/0376-7388(94)87031-4).
- [28] Y. Lanteri, P. Fievet, C. Magnenet, S. Déon, A. Szymczyk, Electrokinetic characterisation of particle deposits from streaming potential coupled with permeate flux measurements during dead-end filtration, *J. Membr. Sci.* 378 (2011) 224–232, <https://doi.org/10.1016/j.memsci.2011.05.002>.
- [29] S.A. Creber, J.S. Vrouwenvelder, M.C.M. van Loosdrecht, M.L. Johns, Chemical cleaning of biofouling in reverse osmosis membranes evaluated using magnetic resonance imaging, *J. Membr. Sci.* 362 (2010) 202–210, <https://doi.org/10.1016/j.memsci.2010.06.052>.
- [30] A. Yeo, P. Yang, A. Fane, T. White, H. Moser, Non-invasive observation of external and internal deposition during membrane filtration by X-ray microimaging (XMI), *J. Membr. Sci.* 250 (2005) 189–193, <https://doi.org/10.1016/j.memsci.2004.10.035>.
- [31] E. Le Ru, P. Etchegoin, *Principles of Surface-Enhanced Raman Spectroscopy: and Related Plasmonic Effects*, Elsevier Science and Technology Books, Inc, n.d. [https://uclibraries.skillport.com/skillportfe/main.action?assetid=RW\\$32695:ss\\_book:37317#summary/BOOKS/RW\\$32695:ss\\_book:37317](https://uclibraries.skillport.com/skillportfe/main.action?assetid=RW$32695:ss_book:37317#summary/BOOKS/RW$32695:ss_book:37317) (accessed May 24, 2020).
- [32] L.F. Greenlee, D.F. Lawler, B.D. Freeman, B. Marrot, P. Moulin, Reverse osmosis desalination: water sources, technology, and today's challenges, *Water Res.* 43 (2009) 2317–2348, <https://doi.org/10.1016/j.watres.2009.03.010>.
- [33] T. Yu, L. Meng, Q.-B. Zhao, Y. Shi, H.-Y. Hu, Y. Lu, Effects of chemical cleaning on RO membrane inorganic, organic and microbial foulant removal in a full-scale plant for municipal wastewater reclamation, *Water Res.* 113 (2017) 1–10, <https://doi.org/10.1016/j.watres.2017.01.068>.
- [34] H.J. Kim, A.E. Fouda, K. Jonasson, In situ study on kinetic behavior during asymmetric membrane formation via phase inversion process using Raman spectroscopy, *J. Appl. Polym. Sci.* 75 (2000) 135–141, [https://doi.org/10.1002/\(SICI\)1097-4628\(20000103\)75:1<135::AID-APP15>3.0.CO;2-9](https://doi.org/10.1002/(SICI)1097-4628(20000103)75:1<135::AID-APP15>3.0.CO;2-9).
- [35] N. Prieto-Taboada, O. Gómez-Laserna, I. Martínez-Arkarazo, M.Á. Olazabal, J.M. Madariaga, Raman spectra of the different phases in the CaSO<sub>4</sub>–H<sub>2</sub>O system, *Anal. Chem.* 86 (2014) 10131–10137, <https://doi.org/10.1021/ac501932f>.
- [36] D. Hasson, R. Semiat, Scale control in saline and wastewater desalination, *Israel Journal of Chemistry*. 46 (2006) 97–104, <https://doi.org/10.1560/BM6M-01UJ-CNP2-WOE3>.